Numerical Study on Swimming Performance Based on Flapping Orientations of Caudal Fins for Bio-robotic Systems

Srikanth Dharwada†
Machine Design Department
IIT Madras
Chennai
dharwadasrikanth@gmail.com

Santhosh Ravichandran†
Machine Design Department
IIT Madras
Chennai

Prabhu Rajagopal†
Machine Design Department
IIT Madras
Chennai
prajagopal@iitm.ac.in

Vishal Hingole†
Machine Design Department
IIT Madras
Chennai

ABSTRACT

Set in the context of the development of bio-inspired robotics systems, this paper seeks to understand the influence of the choice of the flapping orientation of fins on the propulsive performance of small underwater vehicles. In particular, the thunniform mode of Body and/or Caudal Fin (BCF) propelled systems is studied. This research is motivated by the fact that not much literature is available on the influence of flapping orientation of marine organisms and a number of mechanisms are found in nature. Dorso-ventral flapping with a positive metacentric height is shown to yield better self-stabilizing effects and lesser energy consumption compared to sideways flapping. Moreover, with dorso-ventral flapping, the choice of metacentric height could lead to the possibility of adjusting the body's rotational oscillation amplitudes to positively affect the downstream fluid interactions for the caudal fin. This is not possible with sideways flapping where the designer would be forced to change the flapping kinematics or the body shape in the sagittal plane, to adjust the body oscillation amplitudes. While the main body of results are obtained using simulations for underwater vehicle dynamics with coefficients of the REMUS underwater vehicle, stability analysis for a generalised case is also presented.

CCS CONCEPTS

Underwater robotics

AIR '19 02-06 July 2019 Chennai, India

https://doi.org/10.1145/3352593.3352670

KEYWORDS

Bio-inspired underwater robotics; Caudal fin flapping orientation; underwater vehicle dynamics

1 INTRODUCTION

Remotely operated and automated robotic submersibles are today widely used for applications such as inspection, intervention and exploration. As with other fields, there is a growing interest in bio-inspired and bio-mimetic concepts for various elements of submersibles, including propulsion. Bio-inspired propulsion has advantages including efficiency, ability to navigate in complex environments, and is particularly attractive for applications needing stealth. For example, studies of ecological habitats of marine organisms and naval expeditions would benefit from minimally intrusive bio-inspired propulsion. Set in this context, this paper explores the relationship of the flapping orientation of bio-inspired fin-like propulsion systems on the swimming performance of small underwater submersibles, a topic not widely studied in the literature. This research supplements recently published work from the authors' research group on the mechanics of bioinspired caudal fin propulsion for small remotely operated vehicles [1].

Cetaceans, sirenians, phocids and other marine mammals have adopted dorso-ventral oscillations of their caudal propulsors for propulsion. On the other hand, fishes and some swimming reptiles use sideways oscillations of their caudal propulsors or body undulations for propulsion. The reason for such a difference in flapping orientation in nature is perhaps because of the secondary evolution of aquatic mammals while moving from land to water. Initially, terrestrial mammals evolved to realign their limbs from a primitive tetrapod configuration for efficient cursorial movement

on land [2]. Some species of such mammals, while moving to water, evolved towards lift-based propulsion for efficient swimming by going through phases of paddling gaits with their quadruped limbs that eventually evolved to dorso-ventral flapping of caudal flukes [3]. Therefore, there does not seem to be any evidence of performance-driven reasons for different flapping orientations in marine species, which is rather attributed to their differing evolutionary paths.

Aspects of stability and manoeuvrability have been studied extensively in the context of marine vehicles and also to some extent in fishes and mammals [4]. In general, fishes and aquatic mammals have their center of mass above the center of buoyancy due to the distribution of heavier tissues on the dorsal side (or the ventral position of swim bladder in some species [4]. Although this is intrinsically unstable, fishes counteract this instability by producing corrective forces with their fins. However, in man-made systems, it is desirable to have a positive metacentric height [5] i.e. the center of mass positioned below the center of buoyancy to avoid complexity in control and to reduce power consumption [6]. In doing so, for biomimetic caudal fin propelled underwater vehicles, the dynamics of such a mass distribution would be different for dorso-ventral and sideways flapping. A positive metacentric height for the vehicle yields stiffness in the pitching axis which could interact with the moments from dorso-ventral flapping. This is not the case in sideways flapping as the forces and moments are not aligned with the pitching axis. The effects of this principle are discussed in detail in this paper. We identify that the choice of flapping orientation for a biomimetic vehicle could have an impact on its stability and thereby the swimming performance.

Here we investigate the effects of the choice of flapping orientation using underwater dynamics simulations with the body dynamic model of an Autonomous Underwater Vehicle (AUV) (for more details, please see section 2). In our numerical model, the conventional rotary thruster is replaced with a bio-inspired flapping propulsor. Hence, the analysis is limited to thunniform swimming modes for simplicity. Nevertheless, this paper will serve to highlight the potential advantages or effects of the choice of flapping orientation on the swimming performance.

The paper is organised as follows. Firstly, the methods section below provides information on the procedure for numerical simulations and analysis. Next, the results section presents the effects of flapping orientation on stability and finally, the paper concludes after a discussion of the results.

2 METHODS

2.1 6-DOF mathematical model.

To simulate the motion of the swimmer in three-dimensional space, the system is solved for the body fixed frame and transformed to the inertial or earth fixed frame. A set of six equations – three to model the linear movements and the rest for rotational movements, govern the dynamics of the system. The kinematic and dynamic model of the system in consideration is similar to the model used [7]. Society of Naval Architects and Marine Engineers (SNAME) (SNAME, 1964) convention is followed throughout this article. In equation (1), vector η represent position (η_1) and orientation (η_2) in the inertial frame; vector v represents the translational and rotational velocities in the body fixed frame. Throughout the article, $x, y, z, \emptyset, \theta, \psi$ represent surge, sway, heave, roll, pitch and yaw respectively and u, v, w, p, q, r represent their velocities. The origin of the body fixed frame is taken to be at the centre of buoyancy.

$$\eta = [x, y, z, \emptyset, \theta, \psi]^T \tag{1a}$$

$$\eta_1 = [x, y, z]^T \tag{1b}$$

$$\eta_2 = [\phi, \theta, \psi]^T \tag{1c}$$

$$v = [u, v, w, p, q, r]^T \tag{1d}$$

The matrices $J_1(\eta_2)$ and $J_2(\eta_2)$ in equation (2) transform linear and angular velocities from a body-fixed coordinate system to the inertial frame coordinate system.

$$[\dot{x}, \dot{y}, \dot{z}]^T = J_1(\eta_1)[u, v, w]^T; \tag{2a}$$

$$[\dot{\phi}, \dot{\theta}, \dot{\psi}]^T = J_2(\eta_2)[p, q, r]^T \tag{2b}$$

Where,

$$J_1(\eta_1) = [\alpha 1 \quad \beta 1 \quad \gamma 1] \tag{3a}$$

$$\alpha 1 = \begin{bmatrix} c(\psi)\, c(\theta) \\ s(\psi)\, c(\theta) \\ -s(\theta) \end{bmatrix} \tag{3b}$$

$$\beta 1 = \begin{bmatrix} -s(\psi)\, c(\emptyset) + c(\psi)\, s(\theta)\, s(\emptyset) \\ c(\psi)\, c(\emptyset) + s(\emptyset)\, s(\theta)\, s(\psi) \\ c(\theta)\, s(\emptyset) \end{bmatrix} \tag{3c}$$

$$\gamma 1 = \begin{bmatrix} s(\psi)\, s(\emptyset) + c(\psi)\, c(\emptyset)\, s(\theta) \\ -c(\psi)\, s(\emptyset) + s(\theta)\, s(\psi)\, c(\emptyset) \\ c(\theta)\, c(\emptyset) \end{bmatrix} \tag{3d}$$

$$J_2(\eta_2) = [\alpha 2 \quad \beta 2 \quad \gamma 2] \tag{4a}$$

$$\alpha 2 = \begin{bmatrix} 1 \\ 0 \\ 0 \end{bmatrix} \tag{4b}$$

$$\beta 2 = \begin{bmatrix} \mathrm{s}(\emptyset)\,\mathrm{t}(\theta) \\ \mathrm{c}(\psi)\,\mathrm{c}(\emptyset) + \mathrm{s}(\emptyset)\,\mathrm{s}(\theta)\,\mathrm{s}(\psi) \\ s(\emptyset)/c(\theta) \end{bmatrix} \tag{4c}$$

$$\gamma 2 = \begin{bmatrix} \mathrm{c}(\emptyset)\,\mathrm{t}\,(\theta) \\ -s\,(\emptyset) \\ \mathrm{c}(\emptyset)/\,\mathrm{c}\,(\theta) \end{bmatrix} \tag{4d}$$

In equation (3) & (4) and in the rest of this document, the symbols *c*, *s* and *t* correspond to cos, sin and tan operators respectively. The following expression defines the rigid body dynamics in 6-degrees of freedom system with respect to the body fixed frame. *X, Y & Z* represent forces in the surge, sway and heave axes, whereas *K, M & N* represent moments along roll, pitch and yaw axes.

$$M_A \dot{v} = [X, Y, Z, K, M, N]^T + \tau^T \tag{5}$$

Where,

$$\begin{aligned} X = {} & -(W-B)s(\theta) + X_{uu}u|u| + \\ & (X_{wq} - m)wq + (X_{qq} + mx_g)q^2 \\ & + (X_{vr} + m)vr + \left(X_{rr} + mx_g\right)r^2 \\ & - my_g pq - mz_g pr \end{aligned} \tag{6}$$

$$\begin{aligned} Y = {} & (W-B)c(\theta)s(\emptyset) + Y_{vv}v|v| + \\ & Y_{rr}r|r| + Y_{uv}uv + \left(Y_{wp} + m\right)wp + \\ & (Y_{ur} - m)ur - mz_g qr + \\ & \left(Y_{pq} - mx_g\right)pq + Y_{uu\delta_r}u^2\delta_r \end{aligned} \tag{7}$$

$$\begin{aligned} Z = {} & (W-B)c(\theta)c(\emptyset) + Z_{ww}w|w| + \\ & Z_{qq}q|q| + Z_{uw}uw + \left(Z_{uq} + m\right)uq \\ & + \left(Z_{vp} - m\right)vp + \left(mz_g\right)p^2 \\ & + (mz_g)q^2 + (Z_{rp} - mx_g)rp \end{aligned} \tag{8}$$

$$\begin{aligned} K = {} & K_{pp}p|p| - \left(y_g W - y_b B\right)c(\theta)c(\emptyset) \\ & - \left(z_g W - z_b B\right)c(\theta)s(\emptyset) \\ & - \left(I_{zz} - I_{yy}\right)rp + mz_g wp + mz_g ur \end{aligned} \tag{9}$$

$$\begin{aligned} M = {} & -\left(z_g W - z_b B\right)s(\theta) \\ & -\left(x_g W - x_b B\right)c(\theta)c(\emptyset) + M_{ww}w|w| \\ & + M_{qq}q|q| + \left(M_{rp} - (I_{xx} - I_{zz})\right)rp \\ & + mz_g vr - mz_g wq + \left(M_{uq} - mx_g\right)uq \\ & + M_{uw}uw + (M_{vp} + mx_g)vp \end{aligned} \tag{10}$$

$$\begin{aligned} N = {} & -\left(x_g W - x_b B\right)c(\theta)s(\emptyset) \\ & -\left(y_g W - y_b B\right)s(\theta) + N_{vv}v|v| + \\ & N_{rr}r|r| + N_{uv}uv + \left(N_{pq} - \left(I_{yy} - \right.\right. \\ & \left.\left. I_{xx}\right)\right)pq + \left(N_{wp} - mx_g\right)wp + (N_{ur} + \\ & mx_g)ur + N_{uu\delta_r}u^2\delta_r \end{aligned} \tag{11}$$

$$\begin{aligned} \tau = {} & [\,\left|X_{prop}\,s(2\pi t)\right|, Y_{prop}\,s(2\pi t) + \\ & Y_{dist}, Z_{prop}\,s(2\pi t), K_{prop}, \\ & M_{prop}\,s(2\pi t), \;\; N_{prop}\,s(2\pi t)\,] \end{aligned} \tag{12}$$

$$M_A = [\alpha 3 \quad \alpha 4 \quad \beta 3 \quad \beta 4 \quad \gamma 3 \quad \gamma 4] \tag{13a}$$

Where,

$$\alpha 3 = [(m - X_{\dot{u}}) \quad 0 \quad 0 \quad 0 \quad mz_g \quad -my_g]^{\mathrm{T}} \tag{13b}$$

$$\alpha 4 = \left[0 \quad (m - Y_{\dot{v}}) \quad 0 \quad -mz_g \quad 0 \quad \left(mx_g - N_{\dot{v}}\right)\right]^{\mathrm{T}} \tag{13c}$$

$$\beta 3 = \left[0 \quad 0 \quad (m - Z_{\dot{w}}) \quad my_g \quad \left(-mx_g - M_{\dot{w}}\right) \quad 0\right]^{\mathrm{T}} \tag{13d}$$

$$\beta 4 = [0 \quad -mz_g \quad my_g \quad (I_{xx} - K_{\dot{p}}) \quad 0 \quad 0]^T \tag{13e}$$

$$\gamma 3 = [mz_g \quad 0 \quad -Z_{\dot{q}} \quad 0 \quad (I_{yy} - M_{\dot{q}}) \quad 0]^T \tag{13f}$$

$$\gamma 4 = [-my_g \quad (mx_g - Y_{\dot{r}}) \quad 0 \quad 0 \quad 0 \quad (I_{zz} - N_{\dot{r}})]^T \tag{13g}$$

Equation (5) is solved for $\dot{v}$ along with equation (2) for v and then for η with the 'ode15s' function of MATLAB (MATLAB. *R2014a*. (The MathWorks Inc., 2014)).

M_A in the LHS of equation (5) consists of the inertia and added mass terms. The first term in the RHS consists of contributions from cross-flow, centrifugal, coriolis, fin lift, hydrostatic and drag terms, whereas the second term of the RHS consists of forces acting on the body including propulsion forces and external perturbations. Dorso-ventral flapping is modelled by assigning zero to Y_{prop} and N_{prop} in equation (12) and sideways flapping is modelled without Z_{prop} and M_{prop}. The fin lift terms are included only in the sway and yaw equations (equations (8) & (11)) as only rudder control was simulated in this study (to correct the vehicle to swim in a straight line in sideways flapping cases). Also, the propulsive forces assumed to be sinusoidal in nature, based on the results from [8] where thrust and lateral forces are shown to be nearly sinusoidal. The values of these forces, along with other parameters and non-linear coefficients are listed in Table 1.

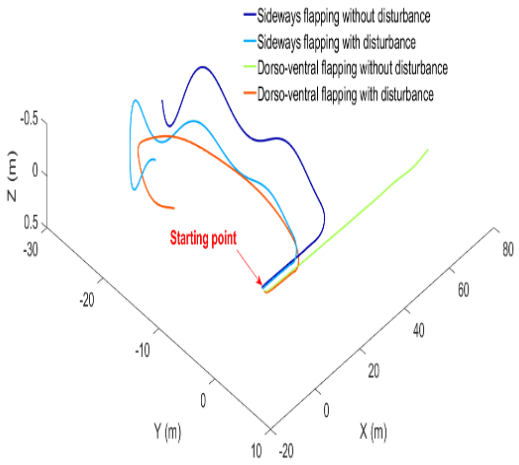

3 RESULTS

Numerical six degrees of freedom (DOF) simulations for underwater vehicle dynamics were performed with the body dynamic coefficients of REMUS underwater vehicle [7]. REMUS is symmetric about two planes (XZ and XY, see Figure 1) with similar body dynamic parameters for both flapping orientations, therefore allowing a fair comparison. The directions of dorso-ventral and sideways flapping axes are indicated in Figure 1.

3.1 Stability of test model

To test the self-stability (stability without active control inputs) of the vehicle against external disturbances such as ocean currents and collisions, a force of 10 N was applied in the sway direction (positive Y, see Figure 1) while the vehicle is swimming forward for a short time period. Studies of disturbances in the heave direction yielded similar results for both flapping orientations. Simulation results of the path of the vehicle with different axes of flapping under these conditions are presented in Figure 2. Interestingly, with sideways flapping, even without any external disturbances, the swimmer seems to tend to a circular path. However, under the same conditions, the swimmer with dorso-ventral flapping behaves as expected, taking a straight-line path without a disturbing force and a circular path with disturbance. It is also interesting to note that, in all these cases, once the vehicle starts tracing a circular path, it continues to do so indefinitely. This behaviour is explained in Figure 3.

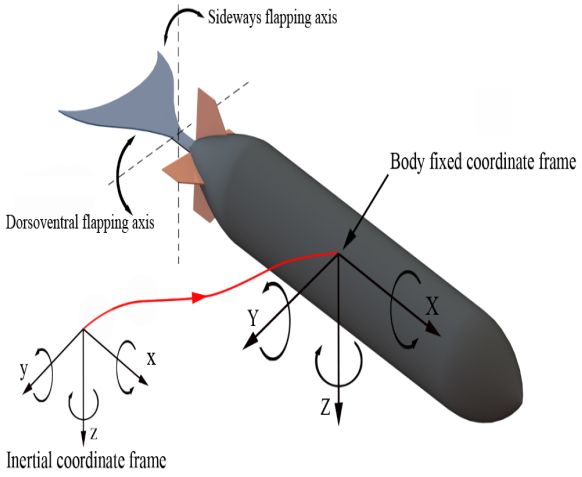

Figure 1: The model used for numerical analysis. Illustration of the model considered for simulations along with its coordinate frames indicating positive directions of linear and rotational axes. The model shown here represents dorso-ventral flapping.

(a) Isometric Model

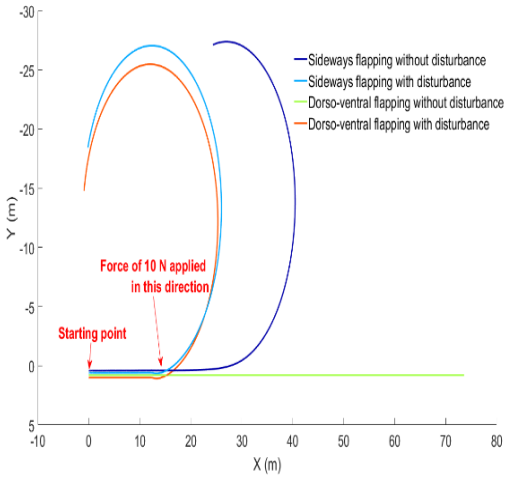

(b) Top View

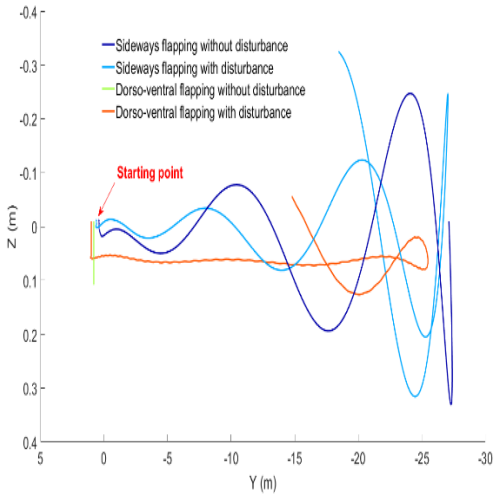

(c) Front View

Figure 2: Simulated paths of the two different flapping orientations. Simulated path of the AUV to compare stability of dorso-ventral flapping and sideways flapping with and without disturbance. A disturbing force of 10 N was applied for 1 second after 36 seconds of forward swimming (in +X direction) which is at about X ~ 10 m in these plots. (a), (b) and (c) shows the path of the AUV in isometric, top and front views respectively.

The cause for motion in a circular path is the sway/yaw coupling of the body. A positive velocity in the sway direction (+*v*) along with a positive forward velocity (+*u*) causes the vehicle to turn in

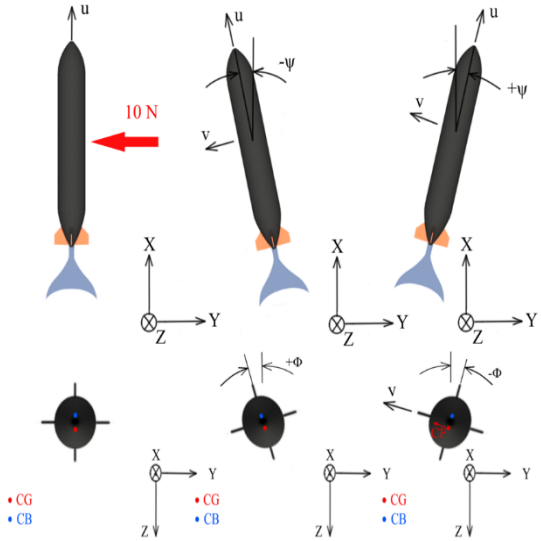

negative direction of the yaw axis. This is because of the cross-flow term which, in this case, is more dominated by the characteristics of the body than the rudder. On the other hand, acceleration in the sway direction will cause the body to turn in the positive direction of yaw axis because of the added mass term being dominant from the rear portion of the body and rudder fins. This said, the physics of such circling behaviour can be explained by breaking down the sequence of events:

i. While the swimmer is moving with a forward velocity, a force of 10 N was applied on the origin of the body coordinate frame for 1 second in the +Y direction (see Figure 3 (a)).
ii. This force causes the vehicle to accelerate in the +Y direction with velocity, *v*. This acceleration in turn causes the vehicle to turn in the positive yaw direction due to the aforementioned crossflow term (see Figure 3 (b)). This rotation attenuates with low accelerations. Also, since the location of the force application is above the center of gravity (CG), the body rolls slightly in the positive direction (see Figure 3 (b)). In the case of a swimmer with sideways flapping, an initial drift in the direction of the Y axis due to initial flapping gives a non-zero value of velocity, *v* in the Y direction.
iii. After the period of acceleration, cross-flow terms begin to dominate. As the velocity *v* grows, the body is rotated in the negative direction of yaw due to the cross-flow torque. This is illustrated in Figure 3 (c).

iv. A rotation in the yaw axis while moving forward yields a curved path. The body also rolls to a negative roll angle due to torque from the centrifugal force on the centre of gravity (see Figure 3 (c)) from the resulting curved path.

v. However, continuation in such a curved path needs a constant torque in the yaw direction. This is given by the generation of sway velocity, *v* due to the centrifugal force. A non-zero sway velocity along with a forward velocity again leads to a negative yawing torque with influence from cross-flow terms as said in step (iii) and the vehicle continues a curved path.

vi. Steps (iii)-(v) are repeated indefinitely and the swimmer continues this circular path.

a b c

Figure 3: Schematics to explain instability. Illustration of numerical results through top view and front view of the body while undergoing a swaying force of 10 N. CG represents centre of gravity and CB represents centre of buoyancy. Centre of buoyancy is also the origin of body co-ordinate system. (a) The body is moving in a straight line just before the application of sideways disturbance force, (b) Body accelerating in +Y direction after application of disturbance of 10 N for 1sec, (c) Body changing its direction of yaw due to the effect of the disturbance.

A similar type of motion is known in aircrafts as the spiral mode [9], in which an aircraft would spiral dive towards the ground if a disturbing force is applied. The longitudinal oscillation observed in Figure 2 is also because of the cross-flow terms resulting from velocities in the surge and heave directions (X and Z respectively) similar to the phugoid mode [9] in aircrafts. However, in this case, a restoring torque due to longitudinal stability (from positive metacentric height) of the vehicle limits this value from growing indefinitely. Figure 4 shows the paths for a vehicle with dorso-ventral flapping of different values of metacentric height (z_g) and a disturbing force applied in the sway direction. Also, as the metacentric height tends to zero (blue line in Figure 4) the COM oscillations amplify. This trend is due to the lack of sufficient restoring moment (with decreasing metacentric height) for the swimmer to control the pitching moment generated from the cross-flow term 'M_{uw}'. The case presented here is for a specific body of an AUV.

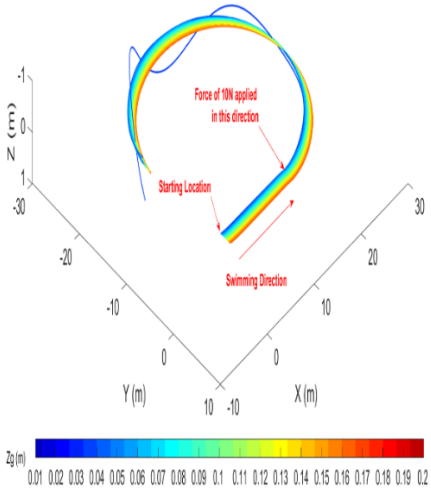

(a) Isometric View

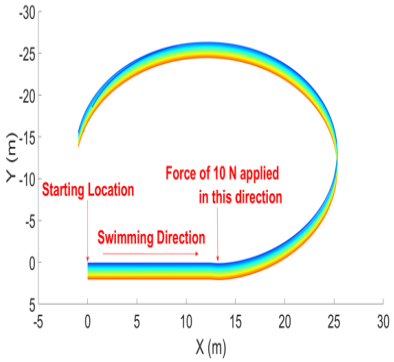

(b) Top View

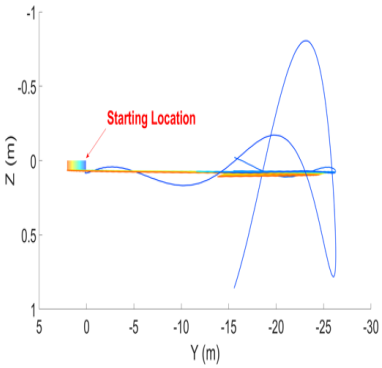

(c) Side View

Figure 4: Simulated paths of a dorso-ventral flapping swimmer at different metacentric heights. Simulated path of the dorso-ventral flapping vehicle with a force of 10 N applied for 1 second after 36 seconds of forward swimming. 'z_g' (shown as 'zg' in the Figure.) in these plots represent the metacentric height. (a), (b) and (c) shows path of the AUV in isometric, top and front views respectively.

For a single case of Dorso-ventral flapping with sideways disturbance the variations in Roll, Pitch and Yaw orientations of the vehicle have been shown in the Figure 5(a). The simulated Surge forces and the Yaw moment acting on the vehicle during the time of flight have been plotted in Figure 5(b). The peak rise in the Sway force (Figure 5(b)), between 20 and 40 secs is because of the simulated disturbance which causes the vehicle to spiral. This disturbance pushes the vehicle in the sway direction leading also to a spike in the yaw moment as described earlier. The oscillation in the pitch and roll plots are due to the offset in the propulsion and disturbance forces relative to the centre of gravity of the vehicle.

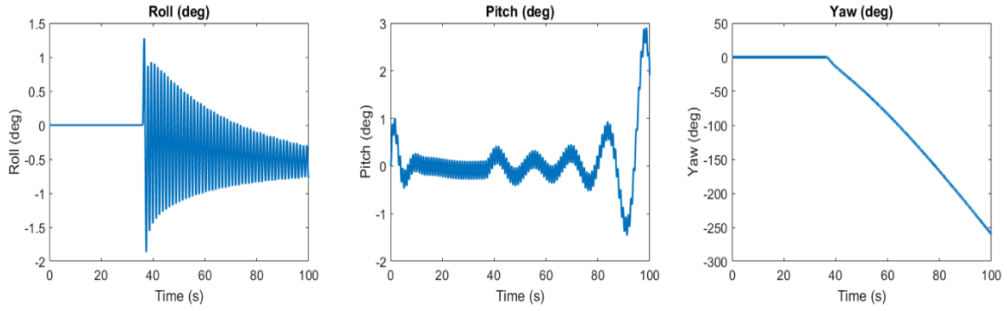

(a)

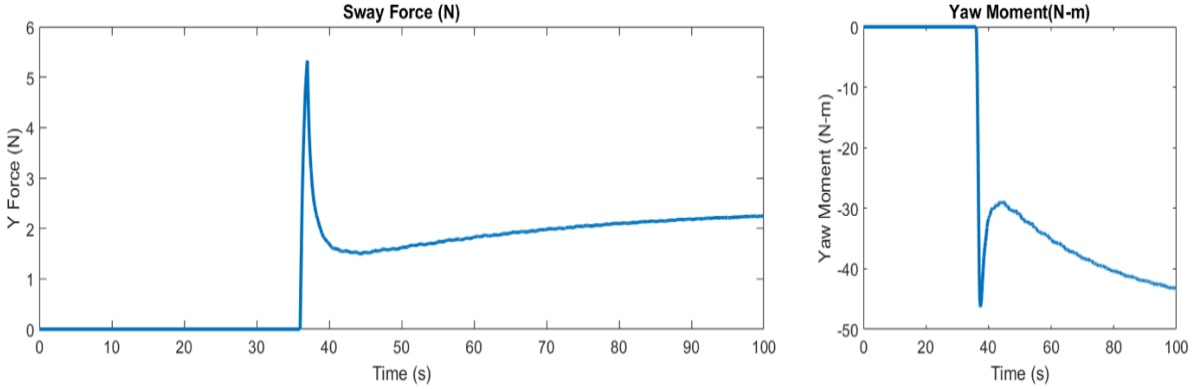

(b)

Figure 5: Simulated orientations and forces acting on the swimmer. (a) Simulated Roll, Pitch and Yaw angles of the swimmer along the path. (b) Simulated Surge force and Yaw moments acting on the swimmer along the path.

4 DISCUSSION

Dorso-ventral flapping swimmers were shown to realize a straight-line path as expected in the absence of a disturbing force, while sideways flapping yields a circular path in the absence of a control input. As most control systems rely on sensory information, a self-stable system would be more reliable even in the case of a sensor failure. For instance, in the event of an inertial measurement unit (IMU) [10] failure, a vehicle with sideways flapping would suffer in even maintaining a straight-line path. This is more important considering that many of the IMUs are unreliable or inaccurate in the yaw axis [11] in the presence of electromagnetic interferences.

In our studies, the propulsive forces were applied on the centre of buoyancy instead of the centre of gravity, which initiated pitch oscillations that were amplified because of cross-flow interactions. If the propulsive force was directly applied on the centre of gravity, the pitching oscillations could have been avoided. However, in practice propulsive forces can rarely be along the centre of gravity. In general, sideways flapping axis cases would have a three-dimensional COM motion (surge, sway and heave) [12] whereas dorso-ventral flapping cases would have it only along two dimensions (surge and heave). It is also interesting to know the effects of an inclined flapping axis generating forces in surge sway and heave similar to the case of a heterocercal caudal fin [13]. Further analysis in this aspect is limited in view of the scope of this article which is primarily to expose differences in performance with different flapping orientations. Nevertheless, this research could open avenues of development through a focus on the analysis of the relationship between centre of mass oscillations and flapping axis orientation on different vehicle models.

5 CONCLUSION

A numerical study on the effects of flapping axis orientation was conducted on thunniform swimming mode, which allowed the idealization to consider an AUV body for the analysis. A self-stable Dorso-ventral flapping was found to advantageous. Limitations of the study and future directions were also discussed in view of the unavailability of existing literature on this topic; for instance, the effect of pressure with respect to depth and assumption of thrust forces to be sinusoidal are a few limitations. Nonetheless, we hope that this study would open avenues of research towards this new area which is totally unexplored.

REFERENCES

[1] A. Krishnadas, S. Ravichandran, and P. Rajagopal, "Analysis of biomimetic caudal fin shapes for optimum propulsive efficiency," *Ocean Eng.*, vol. 153, no. February, pp. 132–142, 2018.

[2] F. E. Fish, "Secondary evolution of aquatic propulsion in higher vertebrates: Validation and prospect," *Integr. Comp. Biol.*, vol. 56, no. 6, pp. 1285–1297, 2016.

[3] F. E. Fish, "Structure and mechanics of nonpiscine control surfaces," *IEEE J. Ocean. Eng.*, vol. 29, no. 3, pp. 605–621, 2004.

[4] P. W. Webb and D. Weihs, "Stability versus maneuvering: Challenges for stability during swimming by fishes," *Integrative and Comparative Biology*, 2015. .

[5] Lewis E.V., *Principles of Naval Architecture, second revision*, vol. II. 1988.

[6] R. D. Christ and R. L. Wernli, *The ROV manual : a user guide to observation-class remotely operated vehicles*. Butterworth-Heinemann, 2007.

[7] T. Prestero, "Development of a six-degree of freedom simulation model for the REMUS autonomous underwater vehicle," in *MTS/IEEE Oceans 2001. An Ocean Odyssey. Conference Proceedings (IEEE Cat. No.01CH37295)*, vol. 1, pp. 450–455.

[8] N. Li, H. Liu, and Y. Su, *Numerical study on the hydrodynamics of thunniform bio-inspired swimming under self-propulsion*, vol. 12, no. 3. 2017.

[9] M. V. Cook, *Flight dynamics primciples. A linear systems approach to aircraft stability and control*. 2013.

[10] M. M. Morrison, Inertial measurement unit. US patent no. US4711125A, Application date: 8th Dec, 1987. URL - https://goo.gl/yZQQNQ

[11] A. R. Jimenez, F. Seco, J. C. Prieto, and J. Guevara, "Indoor Pedestrian navigation using an INS/EKF framework for yaw drift reduction and a foot-mounted IMU," *Proc. 2010 7th Work. Positioning, Navig. Commun. WPNC'10*, pp. 135–143, 2010. URL:https://doi.org/10.1109/WPNC.2010.5649300

[12] G. V Lauder and E. G. Drucker, "Forces, fishes, and fluids: hydrodynamic mechanisms of aquatic locomotion.," *News Physiol. Sci.*, vol. 17, pp. 235–40, Dec. 2002.

[13] G. V Lauder, "Function of the Caudal Fin During Locomotion in Fishes : Kinematics , Flow," *Am. Zool.*, vol. 40, no. January 1999, pp. 101–122, 2000.

Table 1: Nomenclature of the symbols used in the article

Parameters	Value	Units	Description
W	299	N	Weight of the vehicle

B	299	N	Buoyancy of the vehicle
X_{prop}	3.86	N	X-direction thrust due to flapping foil
Y_{prop}	1.93	N	Y-direction force due to flapping foil
Z_{prop}	1.93	N	Z- direction force due to flapping foil
K_{prop}	0	N-m	Roll moment due to flapping foil
M_{prop}	0.115	N-m	Pitch moment due to flapping foil
N_{prop}	0.115	N-m	Yaw moment due to flapping foil
$X_{u\|u\|}$	-1.62e+000	kg/m	Cross-flow Drag
$X_{\dot{u}}$	-9.30e-001	kg	Added Mass
X_{wq}	-3.55e+001	kg/rad	Added Mass Cross-term
$X_{q\|q\|}$	-1.93e+000	kg-m/rad^2	Added Mass Cross-term
X_{vr}	+3.55e+001	kg/rad	Added Mass Cross-term
$X_{r\|r\|}$	-1.93e+000	kg-m/rad^2	Added Mass Cross-term
$Y_{v\|v\|}$	-1.31e+003	kg/m	Cross-flow Drag
$Y_{r\|r\|}$	+6. 32e-001	kg-m/rad^2	Cross-flow Drag
Y_{uv}	-2.86e+001	kg/m	Body Lift Force and Fin Lift
$Y_{\dot{v}}$	-3.55e+001	kg	Added Mass
$Y_{\dot{r}}$	+1.93e+000	kg-m/rad	Added Mass
Y_{ur}	+5.22e+000	kg/rad	Added Mass Cross Term and Fin Lift

Y_{wp}	+3.55e+001	kg/rad	Added Mass Cross-term
Y_{pq}	+1.93e+000	kg-m/rad^2	Added Mass Cross-term
$Z_{w\|w\|}$	-1.31e+002	kg/m	Cross-flow Drag
$Z_{q\|q\|}$	+6.32e-001	kg-m/rad^2	Cross-flow Drag
Z_{wu}	-2.86e+001	kg/m	Body Lift Force and Fin Lift
$Z_{\dot{w}}$	-3.55e+001	kg	Added Mass
$Z_{\dot{q}}$	-1.93e+000	kg-m/rad	Added Mass
Z_{up}	-5.22e+000	kg/rad	Added Mass Cross-term and Fin Lift
Z_{vp}	-3.55e+001	kg/rad	Added Mass Cross-term
Z_{rp}	+1.93e+000	kg-m/rad^2	Added Mass Cross-term
$K_{p\|p\|}$	-1. 30e-001	kg-m^2/rad ^{2}	Rolling Resistance
$K_{\dot{p}}$	-7.04e-002	kg-m^2/rad	Added Mass
$M_{w\|w\|}$	+3.18e+000	kg	Cross-flow Drag
$M_{q\|q\|}$	-1.88e+002	kg-m^2/rad^2	Cross-flow Drag
M_{uw}	+2.40e+001	kg	Body and Fin Lift and Munk Moment
$M_{\dot{w}}$	-1.93e+000	kg-m	Added Mass
$M_{\dot{q}}$	-4.88e+000	kg-m^2/rad	Added Mass
M_{uq}	-2.00e+000	kg-m/rad	Added Mass Cross Term and Fin Lift
M_{vp}	-1.93e+000	kg-m/rad	Added Mass Cross Term

M_{rp}	+4. 86e+000	kg-m^2/rad^2	Added Mass Cross-term
$N_{v\|v\|}$	-3.18e+000	kg	Cross-flow Drag
$N_{r\|r\|}$	-9.40e+001	kg-m^2/rad^2	Cross-flow Drag
N_{uv}	-2.40e+001	kg	Body and Fin Lift and Munk Moment
$N_{\dot{v}}$	+1.93e+000	kg-m	Added Mass
$N_{\dot{r}}$	-4.88e+000	kg-m^2/rad	Added Mass
N_{ur}	-2.00e+000	kg-m/rad	Added Mass Cross Term and Fin Lift
N_{wp}	-1.93e+000	kg-m/rad	Added Mass Cross Term
N_{qp}	-4.86e+000	kg-m^2 /rad^2	Added Mass Cross-term
x_g	+0.0e+000	m	Centre of gravity (x-co-ordinate)
y_g	+0.0e+000	m	Centre of gravity (y-co-ordinate)
z_g	+1.96e-002	m	Centre of gravity (z-co-ordinate)
x_b	+0.0e+000	m	Centre of buoyancy (x-co-ordinate)
y_b	+0.0e+000	m	Centre of buoyancy (y-co-ordinate)
z_b	+0.0e+000	m	Centre of buoyancy (z-co-ordinate)